Design Optimization of the Sensor Spatial Arrangement in a Direct Magnetic Field-Based Localization System for Medical Applications

Luc Maréchal, Shaohui Foong, *Member, IEEE,* Zhenglong Sun, *Member, IEEE* and Kristin L. Wood

Abstract— Motivated by the need for developing a neuro-navigation system to improve efficacy of intracranial surgical procedures, a localization system using passive magnetic fields for real-time monitoring of the insertion process of an external ventricular drain (EVD) catheter is conceived and developed. This system operates on the principle of measuring the static magnetic field of a magnetic marker using an array of magnetic sensors. An artificial neural network (ANN) is directly used for solving the inverse problem of magnetic dipole localization for improved efficiency and precision. As the accuracy of localization system is highly dependent on the sensor spatial location, an optimization framework, based on understanding and classification of experimental sensor characteristics as well as prior knowledge of the general trajectory of the localization pathway, for design of such sensing assemblies is described and investigated in this paper. Both optimized and non-optimized sensor configurations were experimentally evaluated and results show superior performance from the optimized configuration. While the approach presented here utilizes ventriculostomy as an illustrative platform, it can be extended to other medical applications that require localization inside the body.

I. INTRODUCTION

In recent years, passive magnetic field-based sensing systems have been conceived and designed to assist in many medical localization procedures. In such devices, the estimated position of a passive magnetic source is derived from instantaneous magnetic field measurements from a cluster of tri-axis magnetic field sensors. The advantages of this methodology are the simplicity, the cost and the suitability to the medical environment since no external power supply is required to energize the magnetic field of the source. These reasons motivated the design of a system for precise localization during ventriculostmy, a procedure that traditionally is done blind without visual feedback. The system composes of a cylindrical permanent magnet (PM) embedded in an EVD catheter inside the skull and a spatial array of magnetic sensors outside the body. The context and the principle has been described in a previous publication [1].

In many related works, the inverse problem of magnetic dipole localization is solved with the implementation of an algorithm that uses the physics-based dipole model (DM) [2]–[4]. With this approach, the algorithm accuracy is affected by the distortions of the magnetic field due to measurement errors. An alternative is to utilize artificial neural networks (ANNs) to describe and characterize the spatially non-linear magnetic field [5], [6]. An ANN is

L. Maréchal, S. Foong, Z. Sun and K. L. Wood are with the Engineering Product Development Pillar at the Singapore University of Technology and Design, Singapore e-mail: (foongshaohui@sutd.edu.sg).

a computational model that is inspired by the operation of biological neural systems that contain an extensive and massive network of interconnected neurons. In the context of magnetic field-based localization, it provides a model free technique to directly associate and map concurrently measured field measurements by a network of field sensors to position and orientation of the magnetic source. This direct approach, which bypasses the solving of the challenging inverse problem, also has the enhanced advantage of improved localization performance due to the inherent ability of the ANN computational model to naturally compensate for distortion and imperfections during magnetic field sensor measurements.

The PM localization accuracy can be improved by conjointly optimizing: the magnetic sensor itself, the localization algorithm, the number of sensors and the spatial configuration of the sensors. While there has been much analysis concerning the number of sensors on localization performance [7], [8], and optimization of sensors position when using the DM based tracking algorithm [1], so far not much has been reported or presented on the methodology that uses ANNs for direct localization.

Hence, this paper focuses on the influence and effects of spatial arrangement of sensors on localization performance that uses the direct ANN approach. Key advantage of this direct approach is that sensor intrinsic characteristics can be incorporated directly with the ANN. This capability increases the importance and influence of the spatial design of the sensing assembly as certain spatial locations are more advantageous than others. The first step to determine this is to characterize the experimental data of the sensor through a sensor error model and implementing a cost function as described in [9]. This classification and analysis will make it possible to reveal spatial positions where the sensing data provided by the sensor are superior than at others. An experimental validation of the optimization approach is presented by comparing the localization performance of non-optimized and optimized sensor layouts during a typical EVD placement procedure.

II. MATERIALS AND METHOD

For the sensor characterization and analysis, the commercial MAG3110 3-axis magnetic sensor (Freescale, Austin, TX) is chosen due to its high sensitivity and large sensing range. The MAG3110 exhibit a resolution of $0.10 \ \mu$T within a sensing range of $\pm 1000 \ \mu$T. As the spatial location of the sensors play a crucial role in the overall sensing, the following section first characterizes and classifies the experimental

sensing error of the commercial sensor and then uses the result for enhanced spatial design of the sensing assembly.

A. Magnetic Sensor Precision Volumetric Characterization

To quantify and characterize the sensor measurement error, a 6-axis high-precision articulated robotic arm (VS-068, Denso Robotics, Aichi, Japan) is employed. As shown in Figure 1, a grade N52 Neodymium (Nd-Fe-B) magnet with length of 9.5 mm and diameter of 3.2 mm is attached at the end of the end-effector of the arm. The tip of the robotic arm was accurately commanded to specific locations in a discretized 3D volumetric space above a stationary MAG3110 sensor mounted onto the fixed reference frame. This volumetric space is constructed with the origin coinciding with the sensor location and spans x = [0, 26 mm], y = [0, 26 mm], z = [20, 60 mm] and the spacing between adjacent sensing points in the volume is 2 mm. Only a quadrant of the volume above the sensor is characterized because of symmetry of magnetic fields. The robotic arm has a positional repeatability of ± 0.02 mm. The measurements of all 3 axis of the magnetic field sensor, associated with each spatial location, is repeated 10 times. This data at each spatial location is not collected sequentially to avoid measurement bias.

For each point of the mapped space, the precision of the sensor measurement is calculated using the definition of the normalized version of the standard deviation expressed as:

$$STD_{nor_k} = \frac{1}{\bar{\bar{B}}_k} \sqrt{\frac{1}{n-1} \sum_{i=1}^{n} (B_{i,k} - \bar{B}_k)^2} \quad , \qquad (1)$$

$B_{i,k}$ being the value of the magnetic flux density along the k axis (1=x, 2=y, 3=z) of the ith measurement and $\bar{B}_k$ being the arithmetic mean of the n samples considered.

Figure 1 shows the normalized standard deviation of the MAG3110 sensor magnetic flux density values for each point of the mapped space. Larger standard deviations, which has a propensity for poorer localization errors are denoted by larger and lighter circles. As the data suggest, B_x and B_y has a noticeable poorer precision from the higher measurement standard deviation. In particular, B_z shows almost uniform precision throughout the 3D volumetric space while B_x shows significance reduction in precision (or increase in the measurement standard deviation) along the y-axis once a height of $z = 40$ mm is attained.

The data accumulated in Figure 1, enables to build, for each k axis of the sensor, a generalized fitted function which associates a the relative location between the sensor and PM with the measured experimental sensing precision:

$$p_k(x, y, z) = STD_{nor_k} \qquad (2)$$

This relation will then be used in the sensors spatial positioning optimization algorithm that is described further.

B. Sensors Design Optimization

Regarding the ventriculostomy intervention the magnetic field-based sensing device for tracking the EVD catheter will
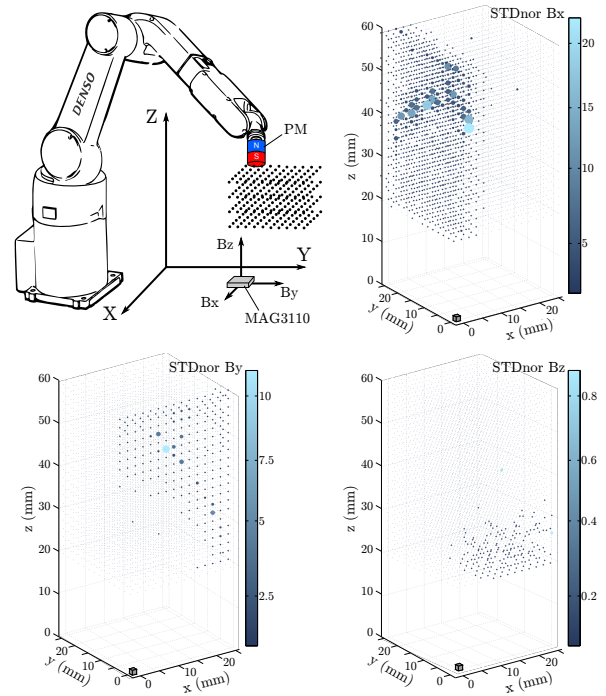

Fig. 1. Mapping of the MAG3110 measurement precision. The PM is positioned by the robotic arm to each discretized point of the 3D space and measuring the magnetic flux density as detected by the sensor. This measurement is done 10 times for each spatial location. On the plots of the normalized standard deviation of B_x, B_y, B_z, the larger the dots the higher the magnitude of the standard deviation.

incorporate a 12 mm hole (to facilitate catheter insertion) within a 40 mm diameter circular area on a planar surface for implementation of the sensors. The sensing device is normal to the skull surface and its origin coincides with the catheter insertion burr hole in the skull. The issue now is how to place the sensors into this planar surface to minimize the effects of the measurement variations as characterized in the previous section. The approach undertaken here is to use reference catheter insertion trajectories and compute the STD_{nor} of the measured field throughout the entire trajectory by placing the sensors on a 1 x 1 mm discretized grid on the planar surface as described in Figure 2. This is applicable because ventriculostomy insertion trajectories are reported in literature with relatively low variance and have been used in the past to evaluate sensor configuration performance [1].

For each possible spatial location on the surface in Figure 2 which denote all possible sensor installation, a penalty fitness value c can be defined for each location as:

$$c(i) = \sum_{j=1}^{n} \sum_{k=1}^{3} p_k(x_j, y_j, z_j) \qquad (3)$$

where i, is the label of the discrete position of the sensors in the sensor planar area. (x_j, y_j, z_j) is the PM position relative to the sensor, along the reference catheter trajectories with a total number of n points. p is the STD_{nor} of the sensor along its k axis calculated as defined in (2). Consequently the best sensor positions are the locations with
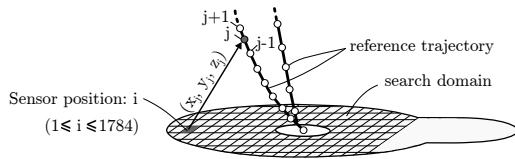
Fig. 2. Evaluating the sensing measurement variation from tracking a reference catheter insertion trajectory at each possible sensor location.
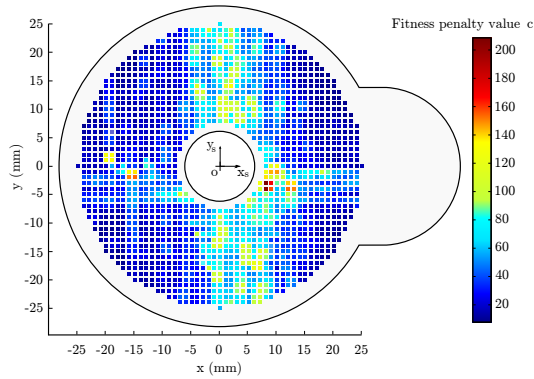

Fig. 3. Fitness penalty value of all possible sensor locations on the sensor board. The grey area is kept clear for the sensors associated electronics on the PCB breakout. O is the origin of the board to be coincident with the burr hole entry point.
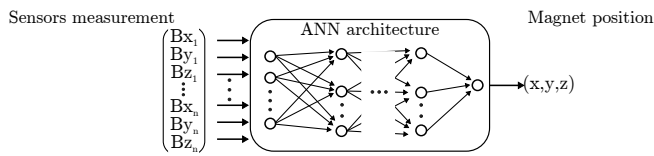

Fig. 4. ANN-based direct magnetic field-based sensing scheme. The sensors data are input in the model and associated to the output (position estimates of the PM) through the neural network.

Fig. 5. Experimental Setup for evaluating optimized and non-optimized sensor arrangements using the 6-axis robotic arm.

low penalty fitness values.

Figure 3 shows the computed penalty fitness value at each possible sensors position on the circular sensor plane. It reveals distinct areas where the penalty fitness values are high (along the y-axis where $x = 0$ mm as well as along the x-axis where $y = 0$ mm) and placement of the sensors at these locations should be avoided as much as possible.

III. EXPERIMENTAL RESULTS

Based on the results illustrated in Figure 3, two distinct sensing systems were designed. One was a non-optimized arrangement where eight sensors are arranged in a regular circular pattern around the insertion hole and an optimized configuration where eight sensors have been specially placed to avoid high penalty fitness values in Figure 3. A visual comparison of both designs are shown in Table I. The sensing mechanism, shown in Figure 4, utilized uses the direct approach of mapping magnetic field measurements directly to position of the PM from the sensor assembly with a 20 hidden network layer ANN. For numerical computation, MATLAB's neural network toolbox (Mathworks, Natick, MA) is used to design and train the ANN for direct sensing.
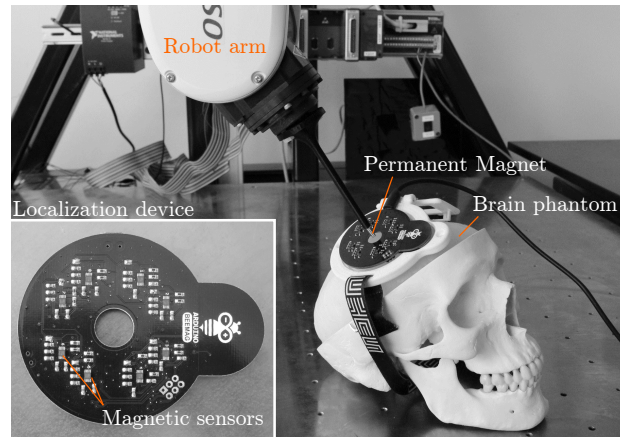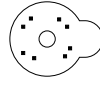
The localization accuracy of both optimally and non-optimally designed systems are evaluated by commanding the robotic arm to replicate four different EVD insertion trajectories composed of 313 points. To achieve this, the following experimental setup that consists of the 6-axis Denso Robot arm, the PM attached to the end-effector, the localization sensor assembly and a custom made brain phantom shown in Figure 5 is used. The brain phantom is made of Ecoflex®0030 (Smooth On Inc, Macungie PA) material and provides a good approximation of the average mechanical behaviour of brain tissues [10]. A microcontroller process the 8 MAG3110 sensors data and communicates with a PC via serial interface.

Figure 6 illustrates the differences between the actual position of the PM (from the robotic arm) and the estimated position from the measurement of the magnetic sensors through the ANN when using the optimized sensor configuration. To quantify the trajectory errors further, the root-mean-squared-error (RMSE) between the observed and estimated positions for both systems are tabulated in Table I. With an RMSE of just 1.0 mm throughout all 4 trajectories, the optimized sensor configuration clearly outperforms the non-optimized layout which has an RMSE of almost double at 1.6 mm. Even the maximum error was significantly lower for the optimized design (at 1.8 mm compared to 4.1 mm).

In addition, from Figure 6, the euclidean error at each position estimate for both sensor designs can be computed and categorized into a histogram. To visualize how well the PM positions are estimated, the distribution of the euclidean error for both sensor designs are consolidated in Figure 7 for direct comparison. As shown in the figure, all the euclidean errors for the optimized sensor configuration are distributed from 0.1 to 1.8 mm. Whereas the distribution for the euclidean error for the non-optimized sensor configuration is much wider, going up all the way to 4.1 mm. This reinforces the superior performance of the optimized sensor layout, which provides significant improvement in sensing performance with no change in the number of sensors used.

TABLE I
LOCALIZATION ACCURACY OVER THE SENSORS CONFIGURATION

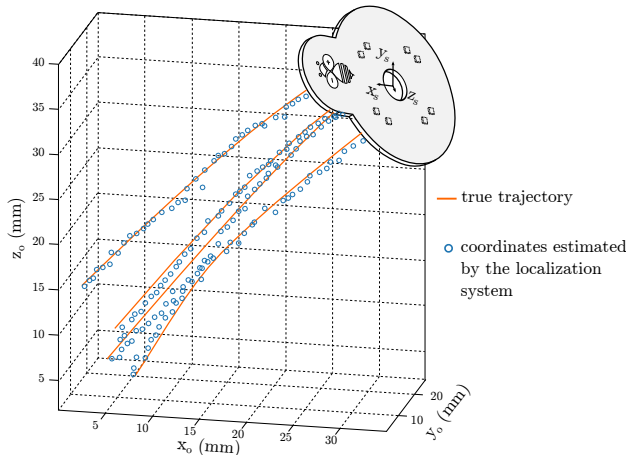| Layout	Non optimized	Optimized
RMSE (mm)	1.6	1.0
Max. Error (mm)	4.1	1.8

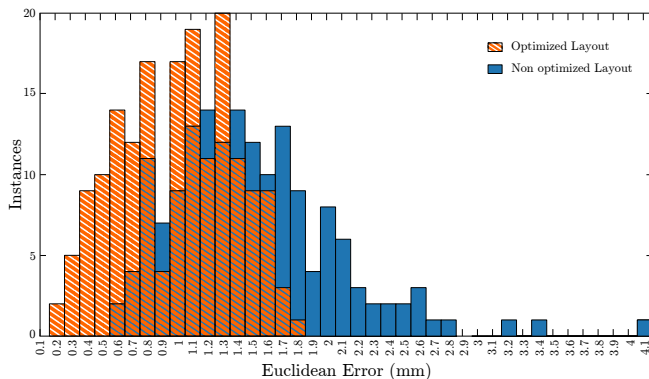Fig. 6. Spatial localization efficiency with four EVD placement paths.

Fig. 7. Distribution of the Euclidean Error throughout the four EVD paths.

IV. DISCUSSION AND CONCLUSION

It is noted that in this paper assumed each sensor in the spatial assembly shared the same intrinsic characteristics in deriving and numerically evaluating the optimal sensor configuration. Of course in real applications, this theoretical assumption will most likely not hold and will inevitably affect the resultant localization performance. This means individual characterization each sensor could potentially and will most likely result in even better localization performance. However experimental results have illustrated that, although this may be true, the effects may not be as significant as the improvements afforded by carefully designing the sensor spatial assembly.

As ventriculostomy is a medical procedure in which the insertion trajectory does not deviate significantly from one patient to another due to the low variance of the location of the ventricles from the burr hole, the design of the sensor spatial configuration can be optimized using a set of reference insertion catheter trajectories with prevalent orientations. However, the framework described can be applied for any other path as well other insertion instruments. Experimental validation have also been conducted *ex vivo* on an anatomical phantom model with representative catheter insertion paths.

From the experimental results and analysis, it is found that compared to blindly adding more sensors, the optimization of the arrangement of the sensors should be of a priority when seeking to enhance localization performance. This finding reiterates the importance of sensor design for magnetic localization system and a sensor design framework based on understanding and classification of the experimental intrinsic characteristics of the sensors was presented and evaluated.

REFERENCES

[1] L. Maréchal, S. Foong, S. Ding, D. Madhavan, K. L. Wood, R. Gupta, V. Patil, and C. J. Walsh, "Optimal Spatial Design of Non-Invasive Magnetic Field-Based Localization Systems," in *IEEE International Conference on Robotics and Automation (ICRA)*, Hong Kong, China, Jun. 2014, pp. 3510–3516.

[2] C. Hu, W. Yang, D. Chen, M. Q. H. Meng, and H. Dai, "An improved magnetic localization and orientation algorithm for wireless capsule endoscope," in *Annual International Conference of the IEEE Engineering in Medicine and Biology Society (EMBC)*, Vancouver, Canada, Aug. 2008, pp. 2055–2058.

[3] D. M. Pham and S. M. Aziz, "A Real-Time Localization System for an Endoscopic Capsule Using Magnetic Sensors," *Sensors*, vol. 14, no. 11, pp. 20 910–20 929, 2014.

[4] Z. Sun, S. Foong, L. Maréchal, T. H. Teo, U.-X. Tan, and A. Shabbir, "Design and analysis of a compliant non-invasive real-time localization system for nasogastric intubation," in *IEEE/ASME International Conference on Advanced Intelligent Mechatronics (AIM)*, Besançon, France, Jul. 2014, pp. 1091–1096.

[5] F. Wu, N. M. Robert, D. D. Frey, and S. Foong, "Enhanced Magnetic Localization with Artificial Neural Network Field Models," in *IEEE International Conference on Robotics and Automation (ICRA)*, Karlsruhe, Germany, May 2013, pp. 1560–1565.

[6] F. Wu, D. D. Frey, and S. Foong, "A hybrid magnetic field model for axisymmetric magnets," in *IEEE/ASME International Conference on Advanced Intelligent Mechatronics (AIM)*, Wollongong, Australia, Jul. 2013, pp. 786–791.

[7] C. Hu, M. Q. Meng, and M. Mandal, "Efficient magnetic localization and orientation technique for capsule endoscopy," in *IEEE/RSJ International Conference on Intelligent Robots and Systems (IROS)*, Edmonton, Canada, Aug. 2005, pp. 628–633.

[8] S. Foong, K.-M. Lee, and K. Bai, "Harnessing Embedded Magnetic Fields for Angular Sensing With Nanodegree Accuracy," *IEEE/ASME Transactions on Mechatronics*, vol. 17, no. 4, pp. 687–696, 2012.

[9] N. Giridhar Singh and M. Joshi, "Optimization of Location and Number of Sensors for Structural Health Monitoring using Genetic Algorithm," *Materials Forum, Annual Review Journal of the Institute of Materials Engineering*, pp. 259–367, 2009.

[10] V. Luboz, E. Promayon, G. Chagnon, T. Alonso, D. Favier, C. Barthod, and Y. Payan, "Validation of a Light Aspiration Device for In Vivo Soft Tissue Characterization (LASTIC)," *Soft Tissue Biomechanical Modeling for Computer Assisted Surgery Studies in Mechanobiology, Tissue Engineering and Biomaterials*, vol. 11, pp. 243–256, 2012.